STEADY-STATE REGULATION OF SECRETORY CARGO EXPORT BY INOSITOL TRISPHOSPHATE RECEPTORS AND PENTA EF HAND PROTEINS

Aaron Held[1], Jennet Hojanazarova[1], John Sargeant[1], Corina Madreiter-Sokolowski[2], Roland Mali[3], Wolfgang F. Graier[3], and Jesse C. Hay[1]

[1]Division of Biological Sciences, Center for Structural & Functional Neuroscience, University of Montana, USA; [2]Department of Health Sciences and Technology, ETH Zürich, Switzerland; [3]Molecular Biology and Biochemistry, Gottfried Schatz Research Center, Medical University of Graz, Austria
correspondence: jesse.hay@umontana.edu

ABSTRACT

ER Ca^{2+} regulates ER-to-Golgi transport machinery. Sustained Ca^{2+} signaling by inositol trisphosphate receptors (IP3Rs) leads to depression of cargo export through activation of penta EF hand protein (PEF) ALG-2 which reduces outer COPII coat at ER exit sites (ERES). However, we do not know whether tonic Ca^{2+} signals during steady-state conditions affect ER export rates and if so by what mechanisms. Here we report that partial depletion of IP3 receptors from NRK epithelial cells causes a marked increase of basal ER export of the transmembrane glycoprotein cargo VSV-G. The increased ER-to-Golgi transport required ALG-2 and was actuated by decreased peflin and increased ALG-2 at ER exit sites (ERES) – a condition previously demonstrated to stimulate COPII-dependent ER export. Upon IP3R depletion the amount of outer coat at ERES increased, the opposite to what occurs during ALG-2-dependent inhibition of secretion during agonist-driven Ca^{2+} signaling. The increased ER export correlated with reduced spontaneous cytosolic Ca^{2+} oscillations caused by the reduced number of Ca^{2+} release channels. IP3R depletion also unexpectedly resulted in partial depletion of ER luminal Ca^{2+} stores. The low Ca^{2+} conditions appeared to decrease both ALG-2 and peflin expression levels somewhat, but these were the only detectable expression changes in COPII trafficking machinery and the Ca^{2+} decrease had no detectable impact on ER stress. We conclude that at steady state, IP3Rs produce tonic Ca^{2+} signals that suppress the basal rate of ER export by maintaining lower outer coat targeting to ERES.

INTRODUCTION

Regulatory roles for Ca^{2+} in intracellular trafficking steps are still being elucidated. Recent work on ER-to-Golgi transport demonstrates involvement of luminal Ca^{2+} stores at a stage following cargo biogenesis and folding/assembly, apparently through the release of Ca^{2+} into the cytoplasm where it binds and activates the vesicle budding, docking and/or fusion machinery (Bentley et al., 2010; Helm et al., 2014). Effector mechanisms by which Ca^{2+} modulates ER-to-Golgi transport appear to involve penta-EF-hand-containing (PEF) protein adaptors that have been implicated in many Ca^{2+}-dependent cellular phenomena (Maki et al., 2002). The PEF protein apoptosis-linked gene-2 (ALG-2) acts as a Ca^{2+} sensor at ER exit sites (ERES) and can stabilize the association of sec31 with the membrane when Ca^{2+} is present (la Cour et al., 2007; Shibata et al., 2010; Shibata et al., 2007; Yamasaki et al., 2006). However, regulation of ER cargo export by ALG-2 and Ca^{2+} does not follow the simple pattern suggested by these early studies. For one thing, ALG-2 in cell extracts exists in a stable heterodimer with another PEF protein - peflin - that binds ALG-2 in a Ca^{2+}-regulated manner (Kitaura et al., 2001; Kitaura et al., 2002) and has been shown to bind ERES through its interactions with ALG-2 to suppress ER export of multiple COPII cargoes (Rayl et al., 2016; Sargeant et al., 2020). For another, release of ALG-2 from peflin appears to change its activity from inhibitory to stimulatory of ER export (Sargeant et al., 2020). Furthermore, sustained agonist-driven Ca^{2+} signaling results in a sharp reduction of ER export that depends entirely on ALG-2 but not on peflin (Sargeant et al., 2020). To summarize, it appears that under sustained signaling conditions ALG-2 has an inhibitory role independent of peflin, but under steady-state conditions has both inhibitory and stimulatory roles modulated by its interactions with peflin.

But what regulates ALG-2 and peflin actions at steady state? Since IP3 receptors, during agonist-driven Ca^{2+} signaling, contribute to PEF protein-mediated regulation of ER export, we wondered whether spontaneous Ca^{2+} signals due to IP3Rs at steady state might also contribute to setting the basal ER export rate. Here we demonstrate that depletion of IP3R-3, the major IP3R isoform in normal rat kidney (NRK) epithelial cells, increases the basal ER export rate of the COPII cargo VSV-G_{ts045} by up to 70% while at the same time causing less frequent spontaneous cytoplasmic Ca^{2+} oscillations and a reduction of ER luminal Ca^{2+} stores. The stimulatory effect on transport is blocked in the absence of ALG-2. The stimulation of

transport is accompanied by a decrease of peflin and increase of ALG-2 and outer coat at ERES. In conclusion, this work indicates that at steady state, spontaneous Ca^{2+} oscillations mediated by IP3Rs favor the inhibitory ALG-2-peflin heterodimer at ERES. Reduction of these tonic signals releases peflin, allowing ALG-2 to stimulate ER export.

RESULTS

Depletion of IP3Rs accelerates ER-to-Golgi transport

To characterize the expression of IP3R isoforms in NRK cells, immunoblotting was performed using antibodies to all three individual IP3R isoforms - IP3R-1, IP3R-2, and IP3R-3. Both IP3R-1 and IP3R-3 were readily detectable in NRK extracts, but IP3R-2 was absent from NRK (data not shown). To determine the ratio of IP3R-1 and IP3R-3 in NRK cells, qRT-PCR was carried out on NRK cell total RNA using isoform-specific primers. As shown in Figure 1A, IP3R-3 was the major isoform, representing 67% of all IP3R subunits; the ratio of IP3R-3:IP3R-1 was thus 2:1 in NRK cells. Using isoform-specific siRNAs, either IP3R-3 or IP3R-1 could be depleted by ~95%, (Figure 1B). IP3Rs form both functional homo-tetramers and functional hetero-tetramers (Stutzmann and Mattson, 2011; Zhang et al., 2011). Hence, IP3R-3 depletion largely eliminated IP3R-3 homo-tetramers and IP3R3-containing hetero-tetramers, leaving only IP3R-1 homo-tetramers, representing about a third of the normal number of channels. Likewise, IP3R-1 depletion left only IP3R-3 homo-tetramers representing about two-thirds of the normal number of total channels. Knockdown of both isoforms was technically feasible, however, this caused cytopathic effects including slow growth and an abnormal ER architecture with swollen ER tubules (not shown). Since it would be difficult to interpret transport changes in the context of this highly abnormal ER, we did not further characterize the complete absence of IP3R channels.

To test the effects of IP3R depletion on ER-to-Golgi cargo transport, we used an intact-cell transport assay (Helm et al., 2014; Rayl et al., 2016; Sargeant et al., 2020; Thayanidhi et al., 2010) employing the temperature-sensitive transmembrane cargo VSV-G_{ts045} to measure the average rate of transport during the first 12 minutes following shift to the transport-permissive temperature of 32 ^{o}C. Figure 1C shows example images and illustrates the morphological principle of the assay. Importantly, as demonstrated quantitatively in Figure 1D, knockdown of

the major IP3R isoform, IP3R-3, resulted in up to a ~70% acceleration of the ER-to-Golgi transport rate. Knockdown of the lesser isoform, IP3R-1, resulted in a less dramatic, though still highly significant, ~20% increase in transport. Taken together these results indicate that under steady-state conditions, both IP3R channel isoforms suppress the rate of ER-to-Golgi transport, roughly in proportion to their abundance. Further characterization of effects of IP3R depletion were carried out only on the dominant IP3R-3 isoform.

Effects of IP3Rs on ER-to-Golgi Transport are mediated by ALG-2

To examine the potential interdependence of IP3Rs and PEF proteins, we combined depletion of IP3Rs with that of ALG-2, a Ca^{2+} effector for ER-to-Golgi transport whose function at ERES is modulated by binding to another PEF protein Ca^{2+} sensor, peflin (Rayl et al., 2016; Sargeant et al., 2020). As demonstrated in the ER-to-Golgi transport assay (Figure 2), IP3R3, by itself, increased transport by ~60%. ALG-2 depletion, by itself, resulted in a ~40% increase in transport. Importantly, when the two knockdowns were combined, transport was increased by only ~30% and was statistically indistinguishable (p=.257) from knockdown of ALG-2 alone. This is the result expected if ALG-2 is required to mediate the increased transport due to IP3R depletion – that ALG-2 is epistatic to IP3Rs. If the two proteins acted independently to suppress transport, the effects of their depletions would have been additive; if the two proteins cooperated, results would have been synergistic.

IP3R depletion causes increased ALG-2 and Sec31A, but decreased peflin targeting to ERES

ALG-2 binds Sec31A at ERES either as an apparent homodimer or as a heterodimer complexed with peflin; while the peflin-lacking species appears to be stimulatory to ER export, the hetero-oligomer with peflin is inhibitory (Kitaura et al., 2001; Sargeant et al., 2020). By immunofluorescence under steady-state DMEM conditions, virtually all ERES positive for ALG-2 are also positive for peflin, and the ratio of the two predicts the rate of cargo export. For example, over-expression of peflin causes more peflin and less ALG-2 at ERES and inhibition of transport while depletion of peflin allows more ALG-2 to bind ERES and results in up to a ~100% increase in transport of COPII-specific cargos at the expanse of bulk flow cargo (Sargeant et al., 2020).

To investigate how ALG-2 drives the transport changes observed when IP3Rs are depleted,

we carried out immunofluorescence of endogenous ALG-2, peflin, and Sec31A on control and IP3R-3-depleted NRK cells. For a non-COPII-related marker of ERES we used rbet1, an ER/Golgi SNARE whose distribution is largely restricted to ERES and ERGIC elements (Hay et al., 1998). Representative images of cells are shown in Figure 3A-C. We segmented the labeling patterns into discrete objects by thresholding and then used Boolean image math to measure the areas of objects and areas of co-localization between objects representing different proteins in the same cell (Rayl et al., 2016; Sargeant et al., 2020). As shown in Figure 3D, when IP3R was depleted, co-localization area between peflin and rbet1 objects decreased by ~25%. The decreased co-localization area was comprised of both a decrease in the percentage of total peflin objects that co-localized with rbet1, and a decrease in the percentage of total rbet1 objects that co-localized with peflin (data not shown); this establishes a true decrease in co-localization that could not result from mere changes in labeling intensity or expression. At the same time, co-localization area between ALG-2 and rbet1 significantly increased by ~35% in IP3R3-depleted cells (Figure 3E). Again, the expanded co-localization area resulted from increases in the percentage of each component's objects that co-localized with the other (data not shown). Focusing on the outer coat, we found that the co-localization area of sec31A and rbet1 increased by ~50% upon IP3R3 depletion (Figure 3F). The expanded co-localization area resulted from increases in the percentage of each component's objects that co-localized with the other (data not shown). The expansion of sec31A-rbet1 overlap most likely indicates that more outer coat was recruited to ERES; this is consistent with past work concluding that ALG-2 'stabilized' the outer coat at ERES (Shibata et al., 2010; Yamasaki et al., 2006). Taken together all immunofluorescence changes during IP3R depletion – decreased rbet1, increased ALG-2 and increased Sec31A recruitment to ERES – predict and/or explain the elevated levels of ER-to-Golgi transport.

IP3R depletion causes reduced spontaneous cytosolic Ca^{2+} oscillations and partial depletion of ER luminal Ca^{2+}

To understand how IP3Rs influence the targeting of ALG-2, peflin and Sec31A at ERES to influence basal secretion rates, we investigated the state of Ca^{2+} homeostasis in IP3R-3-depleted NRK cells. The two-thirds reduction of IP3R channels could cause a reduction in spontaneous Ca^{2+} oscillations due to the fact that Ca^{2+} oscillations depend upon IP3R density

(Thillaiappan et al., 2019). To ascertain whether this was the case in NRK cells, we monitored cytoplasmic Ca^{2+} in NRK cells using the Ca^{2+}-sensitive dye FURA-2. Cells were recorded for 20 min at room temperature in the absence of agonists in extracellular buffer containing 2 mM Ca^{2+}, DMEM vitamins, amino acids and 2 g/L glucose. As shown by representative traces in Figure 4A, cells 2, 4, 5, and 7 displayed episodic Ca^{2+} signaling without agonists present, while cells 1, 3, 6, 8 and 9 did not. Though it was not technically feasible to monitor for longer periods, it is assumed that over longer periods, most NRK cells would display episodes of spontaneous signaling. Furthermore, here we purposefully kept cell density low so as to quantitate the inherent signaling on a per-cell basis. In higher density cultures, such as we normally use for secretion assays, clusters of cells can be observed to oscillate synchronously, presumably due to metabolic coupling through gap junctions, and this effect would be expected to expand the fraction of cells experiencing Ca^{2+} oscillations, as has been reported before in NRK fibroblasts (Almirza et al., 2010). Quantitated data from sparse cells during 10-minute basal recordings is displayed in Figure 4B; each trace was scored as described above as either positive or negative for spontaneous Ca^{2+} oscillations. On average ~22% of sparse, control NRK cells displayed spontaneous Ca^{2+} oscillations whereas ~13% of IP3R3-depleted cells displayed them during the 10-minute interval. These data support the hypothesis that the IP3R-depleted cells display less frequent spontaneous cytosolic Ca^{2+} oscillations.

We also characterized ER luminal Ca^{2+} stores in control and IP3R-depleted cells using D1ER, an ER luminal FRET-based Ca^{2+} sensor (Palmer et al., 2004). The initial, basal FRET ratio, R_0, varied arbitrarily between individual NRK cells - perhaps due to different expression levels and/or sensor aggregation, precluding the ability to directly measure resting Ca^{2+} levels. Therefore all data points, R, were analyzed relative to their initial value, R_0. As shown by representative traces in Figure 4C, upon addition of ionomycin and EGTA to live NRK cells, R/R_0, which for the first five minutes has a value near 1, quickly plunged and approached an R_{min}/R_0 value; R_{min}/R_0 ranged from ~0.75 (for control cells) to ~0.85 (for IP3R-depleted cells). The difference between the initial R/R_0 and R_{min}/R_0, - or $\Delta R/R_0$ - was interpreted to represent the resting ER luminal Ca^{2+} concentration of the cell. As shown in Figure 4D, across many cells in different experiments, $\Delta R/R_0$ was ~28% lower in IP3R-depleted cells. This went against a "common sense" prediction that fewer Ca^{2+} release channels should lead to a build-up of excess luminal Ca^{2+}. To verify the conclusion using a different approach, we used a sarco-

endoplasmic reticulum Ca^{2+} ATPase (SERCA) inhibitor, thapsigargin (Tg), to release ER Ca^{2+}, and then measured the magnitude of the resulting cytoplasmic Ca^{2+} wave in NRK cells transfected with the cytosolic sensor D3cpv (Palmer et al., 2006). As shown in Figure 4E and F, IP3R-depleted NRK cells displayed smaller Ca^{2+} releases, by approximately 33% upon Tg addition, consistent with the conclusion that ER Ca^{2+} stores were partially depleted. We also used a similar Tg addition protocol together with a mitochondrial matrix Ca^{2+} sensor, 4mtcpv (Palmer and Tsien, 2006), and found that mitochondria took up less Ca^{2+} upon release of ER Ca^{2+} in IP3R-depleted cells (data not shown). These experiments indicate that, for reasons that are not obvious, depletion of IP3Rs in NRK cells results in partial depletion of ER Ca^{2+} stores. Although speculations on the molecular cause of the Ca^{2+} depletion are offered in the Discussion, we did not pursue its mechanism further.

Partial depletion of ER luminal Ca^{2+} stores, per se, does not cause acceleration of ER-to-Golgi transport

A reasonable interpretation is that the reduced spontaneous cytosolic Ca^{2+} transients documented in Figure 4B drive the ERES changes displayed in Figure 3 which cause the increased secretion established in Figure 1. The reduced luminal Ca^{2+} would be predicted to contribute to this mechanism but also presents a challenge to the interpretation, since it cannot be eliminated that the reduced luminal store, per se, somehow regulates the transport machinery by an unknown mechanism, perhaps involving luminal Ca^{2+}-binding proteins. If this were the case, comparably reduced luminal Ca^{2+} stores would still stimulate transport, even without depletion of IP3Rs and reduced cytosolic Ca^{2+} oscillations. We experimentally created such a condition by treating cells with very low levels of Tg, two orders of magnitude below the concentrations typically used to induce the unfolded protein response (UPR). As shown in Figure 5A and B, 6 nM Tg for 24 hours resulted in partial depletion of luminal Ca^{2+} similar to that caused by IP3R3 siRNA, while at 10 nM, the Tg caused greater depletion. We then tested the effects of these partial ER Ca^{2+} depletions on ER-to-Golgi transport. As shown in Figure 5C, there were no significant effects on transport at 6 nM Tg, but ~20% inhibition of transport became apparent at 10 nM Tg. Inhibition of ER-to-Golgi transport under conditions of strong ER depletion is expected from previous results, wherein up to 40% inhibition of transport was observed after ER Ca^{2+} was reduced by 85%, from the resting value of ~386 μM, to ~56 μM

(Bentley et al., 2010; Helm et al., 2014). The lack of transport effects at 6 nM demonstrates that partial luminal Ca^{2+} depletion, per se, does not drive the increased transport observed in IP3R-depleted cells. The fact that transport did not increase *at all* was perhaps unexpected, however, it is important to consider that any Ca^{2+} released by IP3Rs in this condition, though perhaps less than normal, may have a greater cytosolic residence time and greater impact on the transport machinery due to the lower SERCA activity in Tg-treated cells. In conclusion, the data favor the interpretation that lowered spontaneous cytosolic Ca^{2+} oscillations, and not the lowered Ca^{2+} store, primarily drives the PEF protein changes that result in increased transport when IP3Rs are depleted.

IP3R depletion down-regulates PEF protein expression but does not alter expression of other trafficking machinery

It was important to know whether IP3R depletion caused increased transport by virtue of increased expression of trafficking machinery, as opposed to by direct Ca^{2+} action at ERES. In particular, one could imagine that lowered ER Ca^{2+} could result in UPR activation which is known to increase expression of COP II-related components. We first examined relevant gene expression using qRT-PCR. As shown in Figure 6A, IP3R-3 knockdown did not significantly affect mRNA expression of COPII inner coat components sec24A, B, C, or D, nor outer shell component sec31A, nor ERES scaffolds sec16A and B. There was perhaps a trend toward an increase of sec24C, but it was not statistically significant and not supported by immunoblotting of cell extracts (see below). Overall, the qRT-PCR data did not support general up-regulation of ERES components as would be expected if basal UPR signaling were higher. In addition, we found that none of the UPR-related genes ATF6, CHOP (labeled "DDIT") or Grp78 (labeled "HspA5") were affected by IP3R depletion. We found that ALG-2 (labeled "PCD6") and peflin (labeled "PEF1") were expressed at very similar levels and not affected by IP3R depletion, at least at the transcript level. Finally, Bcl-2 transcripts were reduced by a significant ~30% upon IP3R depletion; this demonstrates that reduced ER Ca^{2+} stores had the expected homeostatic effect on a Ca^{2+}-regulated gene. We complimented this analysis with immunoblotting of NRK cells extracts transfected with control or IP3R-3 siRNAs. As seen in Figure 6B, UPR mediators phospho-EIF2α, phospho-IRE-1 and ATF4 did not noticeably change upon IP3R depletion. Turning to the transport machinery, Figure 6C demonstrates no

changes in coat subunits sec31A, ß-COP, sec24c, sec23, the ER/Golgi tether p115, cargo receptors ERGIC-58 (labeled "p58") and p24. These results indicate that IP3R depletion did not increase transport by increasing the expression of the required transport machinery. However, we also observed in immunoblots a consistent decrease in both ALG-2 and peflin. This effect was quantified from multiple biological and technical replicates and displayed in Figure 6D, revealing a ~25% decrease in both proteins. Since mRNA levels were not affected (Figure 6A), it appears that this change occurs via a post-translational mechanism. Notably, both proteins are unstable when not in the ALG-2-peflin heterodimer (Kitaura et al., 2001; Kitaura et al., 2002), so this finding could indicate that the reduced Ca^{2+} environment disfavors the heterodimer, consistent with the decreased peflin and increased ALG-2 at ERES documented in Figure 3. As discussed further below, it possible that this apparent regulation of PEF protein expression, though at the whole-cell level not altering the ALG-2:peflin ratio, somehow results in the altered ratio of ALG-2 and peflin at ERES (Figure 3), increasing the secretion rate (Figure 1). Alternatively, the ratio of the two proteins at ERES may be altered directly through the Ca^{2+}-dependent interactions between ALG-2, peflin, Sec31A, and perhaps other ERES components.

DISCUSSION

Steady-state Ca^{2+} signals regulate the rate of ER-to-Golgi transport

This work elucidates a role for basal IP3R-generated Ca^{2+} signals in setting the rate of ER export by modulating the activities and/or targeting of the PEF proteins ALG-2 and peflin at ERES. The data are most consistent with Ca^{2+} binding to PEF proteins to directly modulate their propensity to bind each other and/or Sec31A. For example, if Ca^{2+} signals cause formation of the heterodimer at the expense of ALG-2 homodimers and/or favor heterodimer over homodimer binding to Sec31A, then no further explanation would be needed to accommodate our observations. However, we also uncovered regulation of peflin and ALG-2 protein abundance that occurs when IP3Rs are depleted. Thus, at this time we cannot distinguish whether Ca^{2+} may instead alter the species at ERES through altered stability or turnover of distinct PEF protein complexes. For example, if Ca^{2+} destabilizes non-heterodimeric ALG-2 and peflin species, this could lead to a higher abundance of heterodimers and thus suppression of secretion. This hypothesis is supported by previous in vitro

observations that heterodimer formation stabilizes both proteins, but is hard to reconcile with the observation by the same authors that high Ca^{2+} causes dissociation of the heterodimer (Kitaura et al., 2001). Our results are also difficult to reconcile with the prevalent concept that high Ca^{2+} favors binding of the ALG-2 homodimer - the presumptive stimulatory species in secretion - to its effectors (Maki and Shibata, 2007). More detailed in vitro binding studies with *both* PEF proteins and Sec31A present at different Ca^{2+} concentrations are needed to understand the functional dynamics we have observed at ERES. Binding studies of the heterodimer to Sec31A have not been reported. In addition, determination of protein turnover rates of individual PEF proteins in cells during different Ca^{2+} conditions would also help clarify the mechanism by which Ca^{2+} oscillations shape the secretory landscape through ALG-2 and peflin.

The complex functional relationship between Ca^{2+} and ER cargo export

Ca^{2+} appears to impact ER-to-Golgi transport at several levels. We have known for 30 years that a substantial ER Ca^{2+} store is required for proper folding and quality control of many, but not all protein cargos (Lodish and Kong, 1990). More recently, Ca^{2+} chelator and SERCA inhibitor studies have indicated that luminal Ca^{2+} is required for ER-to-Golgi transport, per se, independently of cargo biosynthesis and folding (Bentley et al., 2010; Chen et al., 2002; Helm et al., 2014). Under severe luminal Ca^{2+} depletion conditions, COPII buds and unfused vesicles accumulate at ERES, and transport is inhibited by ~ 40% (Helm et al., 2014). It is not known whether ALG-2 and peflin are involved in this requirement for luminal Ca^{2+}, or alternatively whether more fundamental properties, for example ERES biosynthesis/organization or membrane fusion, require a minimal level of luminal Ca^{2+}. On the other hand, it does appear that ALG-2 and peflin are involved in adapting the secretory pathway to Ca^{2+} released from the ER into the cytoplasm during signaling. So far, it appears that these signals act to suppress the rate of transport. During sustained Ca^{2+} signaling, ALG-2 mediates a sharp suppression of ER-to-Golgi transport (Sargeant et al., 2020). Here, we demonstrate that steady-state Ca^{2+} signals mediated by IP3Rs also appear to suppress transport. An important remaining question is whether the modulatory effects of Ca^{2+} at steady state described here are simply a less severe application of the same mechanisms by which ALG-2 sharply curtails ER export during agonist-driven Ca^{2+} signaling. Alternatively, there could be a different targeting principle or

activity of ALG-2 that is activated during continuous high Ca^{2+}. In conclusion, ER Ca^{2+} appears to have several regulatory roles in biosynthetic secretion, one subset of which are inhibitory and mediated through ALG-2 and peflin when Ca^{2+} is released by IP3Rs at steady state.

IP3Rs and the ER Ca^{2+} store

The fact that IP3R depletion caused a reduction of luminal Ca^{2+} is challenging to interpret. A simple interpretation would be that IP3Rs are involved in store-operated Ca^{2+} entry (SOCE) in NRK cells. Indeed, a direct role of IP3Rs in SOCE in *Drosophila* has been demonstrated (Chakraborty et al., 2016); however, their direct role in SOCE in mammalian cells, though widely discussed, is not well-supported (Thillaiappan et al., 2019). Furthermore, IP3R inhibitors such as 2-Aminoethoxydiphenyl borate (2-APB) and xestospongins cannot be conveniently used to clarify the role of IP3Rs in SOCE, or aid in the present studies, since they also inhibit SOCE and SERCA independently of IP3Rs (Stutzmann and Mattson, 2011). As detailed in Figure 5 and 6, control experiments allowed us to determine that changes in luminal Ca^{2+} caused by IP3R siRNAs did not appear to drive the effects we observed on ER-to-Golgi transport.

MATERIALS AND METHODS

Antibodies

Mouse monoclonal anti-mannosidase II antibody was purchased from Covance Research Products (Denver, PA; product MMS-110R-200). Rabbit polyclonal anti-IP3R-1 antibody was purchased from ThermoFisher Scientific (Waltham, MA; product PA1-901). Mouse monoclonal anti-IP3R-3 antibody was purchased from BD Biosciences (San Jose, Ca^{2+}; item 610313). Anti-rbet1 mouse monoclonal antibody, clone 16G6, was as described (Hay et al., 1998). Rabbit polyclonal anti-peflin and chicken polyclonal anti-ALG-2 were produced previously {Sargeant:2020ba}. Rabbit polyclonal anti-sec31A, anti-sec23, anti-p24 and anti-β-Cop were produced previously against synthetic peptides (Bentley et al., 2010; Xu and Hay, 2004). Rabbit polyclonal anti-Phospho-eIF2α antibody was purchased from Cell Signaling Technology (Danvers, MA; product 9721s). Rabbit polyclonal anti Phospho-IRE1 was purchased from Abcam (Cambridge, United Kingdom; item ab48187. Rabbit polyclonal anti-

ATF4 antibody was purchased from GeneTex (Irvine, Ca^{2+}; product GTX101943). Rabbit polyclonal anti-sec24c was a kind gift from Dr. William Balch (Scripps Institute). Rabbit polyclonal anti-p115 was produced in-house (Wang et al., 2015). Rabbit polyclonal anti-p58 was a kind gift from Dr. Jaakko Saraste (University of Bergen, Norway). Secondary antibody congugates with Alexa Flour™ 488 were from Invitrogen (Carlsbad, CA; product A11001). Cy3- and cy5-conjugated secondary antibodies were purchased from Jackson ImmunoResearch Laboratories (West Grove, PA).

qRT-PCR

NRK cells were transfected with IP3R-3 siRNA (see below) using Transfast (Promega Corp.; Madison WI) using manufacturer's instructions. Total RNA was isolated using the PEQLAB total RNA isolation kit (Peqlab; Erlangen, Germany) and reverse transcription was performed in a thermal cycler (Peqlab) using a cDNA synthesis kit (Applied Biosystems; Foster City, CA). mRNA levels were examined by qRT-PCR. A QuantiFast SYBR Green RT-PCR kit (Qiagen; Hilden, Germany) was used to perform real time PCR on a LightCycler 480 (Roche Diagnostics; Vienna, Austria), and data were analyzed by the REST Software (Qiagen). Relative expression of specific genes was normalized to human GAPDH as a housekeeping gene. Primers for real time PCR were obtained from Invitrogen (Vienna, Austria).

siRNA knockdowns and transfections

For transport experiments and Ca^{2+} measurements NRK cells were electroporated with 0.6 µM siRNA and grown in DMEM high glucose containing 10% fetal calf serum and 1% penicillin-streptomycin. After 2-3 days of normal growth at 37 ^{o}C, the cells were resuspended and re-electroporated, this time with a combination of the siRNA plus 7.5 µg of VSV-G-GFP plasmid. Cells were allowed to recover and grow on coverslips at 41 ^{o}C for 24 h. For all non-transport experiments the same protocol was performed, but after specific plasmid transfection, cells were allowed to recover and grown on coverslips at 37 °C.

Alternatively, for the immunofluorescence experiments (Figure 3), sub-confluent cells grown on glass coverslips in 6-well plates were directly transfected without resuspension. After ~16 h incubation in OptiMEM containing 0.3% RNAiMax (Invitrogen; Carlsbad, CA) and 0.28 µM siRNA, transfection medium was supplemented with an equal part of OptiMEM containing

5% fetal calf serum, 2mM $CaCl_2$, and 1% penicillin-streptomycin and incubated for another 3-5 hours. Subsequently, this post-transfection medium was removed (but saved) and replaced with DMEM containing 10% fetal calf serum, 1% penicillin-streptomycin, 0.3% PolyJet (SignaGen Laboratories; Frederick, MD) , and 1 µg/ml plasmid. After ~12 h incubation, the plasmid solution was removed, cells were washed twice with PBS and returned to their siRNA-containing OptiMEM medium to recover while continuing the knockdown for another 24 h.

There was no noticeable difference in knockdown or transfection efficiency between the two transfection protocols. Cells from all transfections were either lysed directly in SDS-PAGE sample buffer for quantitative immunoblotting, or else processed for transport, colocalization, or FRET assays as described below.

Custom siRNAs were purchased from Ambion/Thermo Fisher (Waltham, MA) or Gene Link (Elmsford, NY) and contained no special modifications. We used two different siRNAs for IP3R-3 which appeared to perform similarly in knockdown efficiency and effects on Ca^{2+} and secretion; the large majority of experiments were performed using siRNA Itpr3-7848 (5' GCA GAC UAA GCA GGA CAA A dTdT 3'). siRNA Itpr3-0452 (5' GGA UGU GGA GAA CUA CAA A dTdT 3') was used intermittently for confirmation purposes. ALG-2 siRNA was described and its effects on secretion confirmed previously (Helm et al., 2014; Rayl et al., 2016). Control siRNAs were custom synthesized non-targeting siRNAs from the same manufacturer. Immunoblotting of cell lysates enabled validation of knockdown efficiencies for each siRNA experiment that was functionally analyzed.

ER-to-Golgi transport assay

NRK cells were transfected with plasmid and/or siRNA as described above and plated on Poly-L-lysine coated coverslips. After 24 hours of cargo plasmid expression at 41 ^{o}C, the cells were either fixed by dropping coverslips directly into fixative or into 6-well chambers containing pre-equilibrated 32 ^{o}C medium for 12 min, then transferred to fixative. Coverslips were fixed and labeled using anti-mannosidase II antibody as described in the immunofluorescence section below. Morphological quantitation of ER-to-Golgi transport was accomplished as described previously (Rayl et al., 2016; Sargeant et al., 2020). Briefly, images were collected in a consistent manner with regard to cell morphology, protein expression levels and exposure. A single widefield image plane was collected for each color channel (GFP and

mannosidase II) for each field of cells randomly encountered; image deconvolution was not performed. Images were analyzed using ImageJ open source image software with automation by a custom script (available upon request) that randomizes the images and presents them to the user in a blind fashion. The user identifies transfected cells and subcellular regions while the script extracts parameters including extracellular background, Golgi intensity and diffuse cytoplasmic ER intensity. Transport index is calculated for each individual cell as ($Golgi_{max}$ - background) / (ER_{mean} - background), and all extracted parameters are written to an appendable output file along with a cell number and image title so that the data was traceable. Using this method, the user quantitates about 60 cells per hour. Once transport indices have been obtained for all conditions in an experiment, each value is subtracted by the mean transport index value for cells that were fixed directly from 41 ^{o}C without a transport incubation at 32 ^{o}C (typically a value between 1.0 and 1.5) to generate the net transport index. Net transport indices are then normalized to the mean siControl value for the particular experiment, prior to plotting and comparison between experiments. Each result reported here was obtained in at least three separate experiments on different days.

Immunofluorescence microscopy

Coverslips were fixed with 4% paraformaldehyde containing 0.1M sodium phosphate (pH 7.0) for 30 min at room temperature and quenched twice for 10 min with PBS containing 0.1M glycine. Fixed cells were treated for 15 min at room temperature with permeabilization solution containing 0.4% saponin, 1% BSA, and 2% normal goat serum dissolved in PBS. The cells were then incubated with primary antibodies diluted in permeabilization solution for 1 h at room temperature. Next, coverslips were washed 3x with permeabilization solution and incubated 30 min at room temperature with different combinations of Alexa Flour™ 488-, Cy3-, and/or Cy5-conjugated anti-mouse, anti-rabbit, or anti-chicken secondary antibodies. After the secondary antibody incubation, coverslips were again washed 3x using permeabilization solution and mounted on glass slides using Slow Fade Gold antifade reagent (Invitrogen product S36936) and the edges sealed with nail polish. Slides were analyzed using a 40x or 60x objective on a Nikon E800 widefield microscope with an LED illumination unit (CoolLED pE 300^{white}), sCMOS PCO.edge 4.2 camera, Prior excitation and emission filter wheels and Z-drive, automated using Micro-Manager software.

Colocalization Assays

For immunofluorescence co-localization experiments fixed NRK cells such as in Figure 3 were captured using a 60x/1.40 Plan Apo objective as z-stacks in eleven 200-nm increments for each color channel. Image stacks were deconvolved using Huygens Essential Widefield software (Scientific Volume Imaging, Hilversum, The Netherlands). Final images for display and quantitation represent maximum intensity projections of deconvolved stacks. ERES area was assessed by a custom ImageJ script (available upon request). Briefly, background labeling was removed by defining a dark extracellular area of each channel image as zero. For each cell an object binary image mask (excluding the nucleus) was generated for each individual channel by auto thresholding using the 'Moments' (for rbet1) or 'Renyi Entropy' (for ALG-2, Peflin, and sec31) algorithms. Next, each channel mask was compared to the other using a Boolean 'and' operation to create a co-localization binary mask. The total object area for each mask was extracted and written to an appendable output file along with the cell number and image title so that the data was traceable. Colocalization areas for each cell were then normalized to the mean siControl value for the particular experiment, prior to plotting and comparison as reported in figure 3.

Calcium Imaging

Subconfluent NRK cells growing on glass coverslips were transfected with genetically encoded Ca^{2+} sensors D1ER or D3cpv and siRNA as described above and imaged the next day. In some experiments (Figure 4 A,B) control or knockdown cells were loaded with FURA-2-AM for 40 minutes at room temperature directly prior to imaging, rather than transfection with a Ca^{2+} sensor. Coverslips were placed in a perfusion chamber and perfused with $2Ca^{2+}$ buffer (2 mM $CaCl_2$, 138 mM NaCl, 1 mM $MgCl_2$, 5 mM KCl, 10 mM D-glucose, 10 mM Hepes, pH 7.4) at 2 ml/min at room temperature on a Nikon TE300 inverted microscope equipped with a 40x objective, motorized high speed Sutter Lambda filter wheel for emissions, CoolLED pe340 excitation system, and PCO Panda sCMOS camera, automated with Micro-Manager software. Imaging was carried out using various perfusion protocols as described below with imaging at 3-second intervals. For examination of basal Ca^{2+} oscillations as in Figure 4A and B, cells were labeled with FURA-2 and imaged for 10 (Figure 4B) or 20 (Figure 4A) minutes in $2Ca^{2+}$

buffer. Each imaging interval involved collecting an image at 510 nm emission and 340 or 380 nm excitation. For all other protocols, each imaging interval involved collecting images at 480 nm and 530 nm using 430 nm excitation. For examination of ER luminal Ca^{2+} stores as in Figure 4C, cells were transfected with D1ER and imaged for a total of 12 minutes. After 5 min of $2Ca^{2+}$ buffer, the buffer was changed to $0Ca^{2+}$ buffer (138 mM NaCl, 1 mM $MgCl_2$, 5mM KCl, 10 mM D-glucose, 0.1 mM EGTA, 10 mM Hepes, pH 7.4) + 3 µM Ionomycin. For examination of cytosolic Ca^{2+} release as in Figure 4E, cells were transfected with D3cpv and imaged for a total of 15 minutes. After 5 minutes, the running buffer was changed to $2Ca^{2+}$ buffer + 200nM Thapsigargin (Tg). For analysis in ImageJ, each cell, as well as an extracellular background region was enclosed in an ROI and mean intensity was collected in each color channel at each time interval. Data was imported to Kaleidagraph software, where the intensity data was converted to ratios. For Fura, R= (emission at 510 nm when excited at 340 nm - background at 510/340) / (emission at 510 nm when excited at 380 nm - background at 510/380). For FRET sensors, with excitation at 430 nm, R= (emission at 530 nm - background at 530) / (emission at 480 nm - background at 480). The FRET ratio curves were then converted to R/R_0 by dividing every R value by the initial R value for each trace and, when necessary, fit to a polynomial or exponential decay function to remove effects of progressive photo-bleaching or baseline drift.

REFERENCES

Almirza, W. H. M., Peters, P. H. J., van Meerwijk, W. P. M., van Zoelen, E. J. J. and Theuvenet, A. P. R. (2010). Different roles of inositol 1,4,5-trisphosphate receptor subtypes in prostaglandin F(2alpha)-induced calcium oscillations and pacemaking activity of NRK fibroblasts. *Cell Calcium* **47**, 544–553.

Bentley, M., Nycz, D. C., Joglekar, A., Fertschai, I., Malli, R., Graier, W. F. and Hay, J. C. (2010). Vesicular calcium regulates coat retention, fusogenicity, and size of pre-Golgi intermediates. *Mol Biol Cell* **21**, 1033–1046.

Chakraborty, S., Deb, B. K., Chorna, T., Konieczny, V., Taylor, C. W. and Hasan, G. (2016). Mutant IP3 receptors attenuate store-operated Ca2+ entry by destabilizing STIM-Orai interactions in Drosophila neurons. *J Cell Sci* **129**, 3903–3910.

Chen, J.-L., Ahluwalia, J. P. and Stamnes, M. (2002). Selective effects of calcium chelators on anterograde and retrograde protein transport in the cell. *J Biol Chem* **277**, 35682–35687.

Hay, J. C., Klumperman, J., Oorschot, V., Steegmaier, M., Kuo, C. S. and Scheller, R. H. (1998). Localization, dynamics, and protein interactions reveal distinct roles for ER and Golgi SNAREs. *J. Cell Biol.* **141**, 1489–1502.

Helm, J. R., Bentley, M., Thorsen, K. D., Wang, T., Foltz, L., Oorschot, V., Klumperman, J. and Hay, J. C. (2014). Apoptosis-linked gene-2 (ALG-2)/Sec31 interactions regulate endoplasmic reticulum (ER)-to-Golgi transport: a potential effector pathway for luminal calcium. *J Biol Chem* **289**, 23609–23628.

Kitaura, Y., Matsumoto, S., Satoh, H., Hitomi, K. and Maki, M. (2001). Peflin and ALG-2, members of the penta-EF-hand protein family, form a heterodimer that dissociates in a Ca2+-dependent manner. *J Biol Chem* **276**, 14053–14058.

Kitaura, Y., Satoh, H., Takahashi, H., Shibata, H. and Maki, M. (2002). Both ALG-2 and peflin, penta-EF-hand (PEF) proteins, are stabilized by dimerization through their fifth EF-hand regions. *Arch Biochem Biophys* **399**, 12–18.

la Cour, J. M., Mollerup, J. and Berchtold, M. W. (2007). ALG-2 oscillates in subcellular localization, unitemporally with calcium oscillations. *Biochem Biophys Res Commun* **353**, 1063–1067.

Lodish, H. F. and Kong, N. (1990). Perturbation of cellular calcium blocks exit of secretory proteins from the rough endoplasmic reticulum. *J Biol Chem* **265**, 10893–10899.

Maki, M. and Shibata, H. (2007). The penta-EF-hand protein ALG-2 and its interacting proteins. *Calcium Binding Proteins*.

Maki, M., Kitaura, Y., Satoh, H., Ohkouchi, S. and Shibata, H. (2002). Structures, functions and molecular evolution of the penta-EF-hand Ca2+-binding proteins. *Biochim Biophys Acta* **1600**, 51–60.

Palmer, A. E. and Tsien, R. Y. (2006). Measuring calcium signaling using genetically targetable fluorescent indicators. *Nat Protoc* **1**, 1057–1065.

Palmer, A. E., Giacomello, M., Kortemme, T., Hires, S. A., Lev-Ram, V., Baker, D. and Tsien, R. Y. (2006). Ca2+ indicators based on computationally redesigned calmodulin-peptide pairs. *Chem. Biol.* **13**, 521–530.

Palmer, A. E., Jin, C., Reed, J. C. and Tsien, R. Y. (2004). Bcl-2-mediated alterations in endoplasmic reticulum Ca2+ analyzed with an improved genetically encoded fluorescent sensor. *Proc Natl Acad Sci USA* **101**, 17404–17409.

Rayl, M., Truitt, M., Held, A., Sargeant, J., Thorsen, K. and Hay, J. C. (2016). Penta-EF-Hand Protein Peflin Is a Negative Regulator of ER-To-Golgi Transport. *PLoS ONE* **11**, e0157227.

Sargeant, J., Costain, T., Madreiter-Sokolowski, C. T., Gordon, D. E., Peden, A. A., Malli, R., Graier, W. F. and Hay, J. C. (2020). Calcium Sensors ALG-2 And Peflin Bind ER Exit Sites In Alternate States To Modulate Secretion In Response To Calcium Signaling. *bioRxiv* 2020.02.22.944264.

Shibata, H., Inuzuka, T., Yoshida, H., Sugiura, H., Wada, I. and Maki, M. (2010). The ALG-2 binding site in Sec31A influences the retention kinetics of Sec31A at the endoplasmic reticulum exit sites as revealed by live-cell time-lapse imaging. *Biosci. Biotechnol. Biochem.* **74**, 1819–1826.

Shibata, H., Suzuki, H., Yoshida, H. and Maki, M. (2007). ALG-2 directly binds Sec31A and localizes at endoplasmic reticulum exit sites in a Ca2+-dependent manner. *Biochem Biophys Res Commun* **353**, 756–763.

Stutzmann, G. E. and Mattson, M. P. (2011). Endoplasmic reticulum Ca(2+) handling in excitable cells in health and disease. *Pharmacol. Rev.* **63**, 700–727.

Thayanidhi, N., Helm, J. R., Nycz, D. C., Bentley, M., Liang, Y. and Hay, J. C. (2010). Alpha-synuclein delays endoplasmic reticulum (ER)-to-Golgi transport in mammalian cells by antagonizing ER/Golgi SNAREs. *Mol Biol Cell* **21**, 1850–1863.

Thillaiappan, N. B., Chakraborty, P., Hasan, G. and Taylor, C. W. (2019). IP3 receptors and Ca2+ entry. *Biochim Biophys Acta Mol Cell Res* **1866**, 1092–1100.

Wang, T., Grabski, R., Sztul, E. and Hay, J. C. (2015). p115-SNARE interactions: a dynamic cycle of p115 binding monomeric SNARE motifs and releasing assembled bundles. *Traffic* **16**, 148–171.

Xu, D. and Hay, J. C. (2004). Reconstitution of COPII vesicle fusion to generate a pre-Golgi intermediate compartment. **167**, 997–1003.

Yamasaki, A., Tani, K., Yamamoto, A., Kitamura, N. and Komada, M. (2006). The Ca2+-binding protein ALG-2 is recruited to endoplasmic reticulum exit sites by Sec31A and stabilizes the localization of Sec31A. *Mol Biol Cell* **17**, 4876–4887.

Zhang, S., Fritz, N., Ibarra, C. and Uhlén, P. (2011). Inositol 1,4,5-trisphosphate receptor subtype-specific regulation of calcium oscillations. *Neurochem. Res.* **36**, 1175–1185.

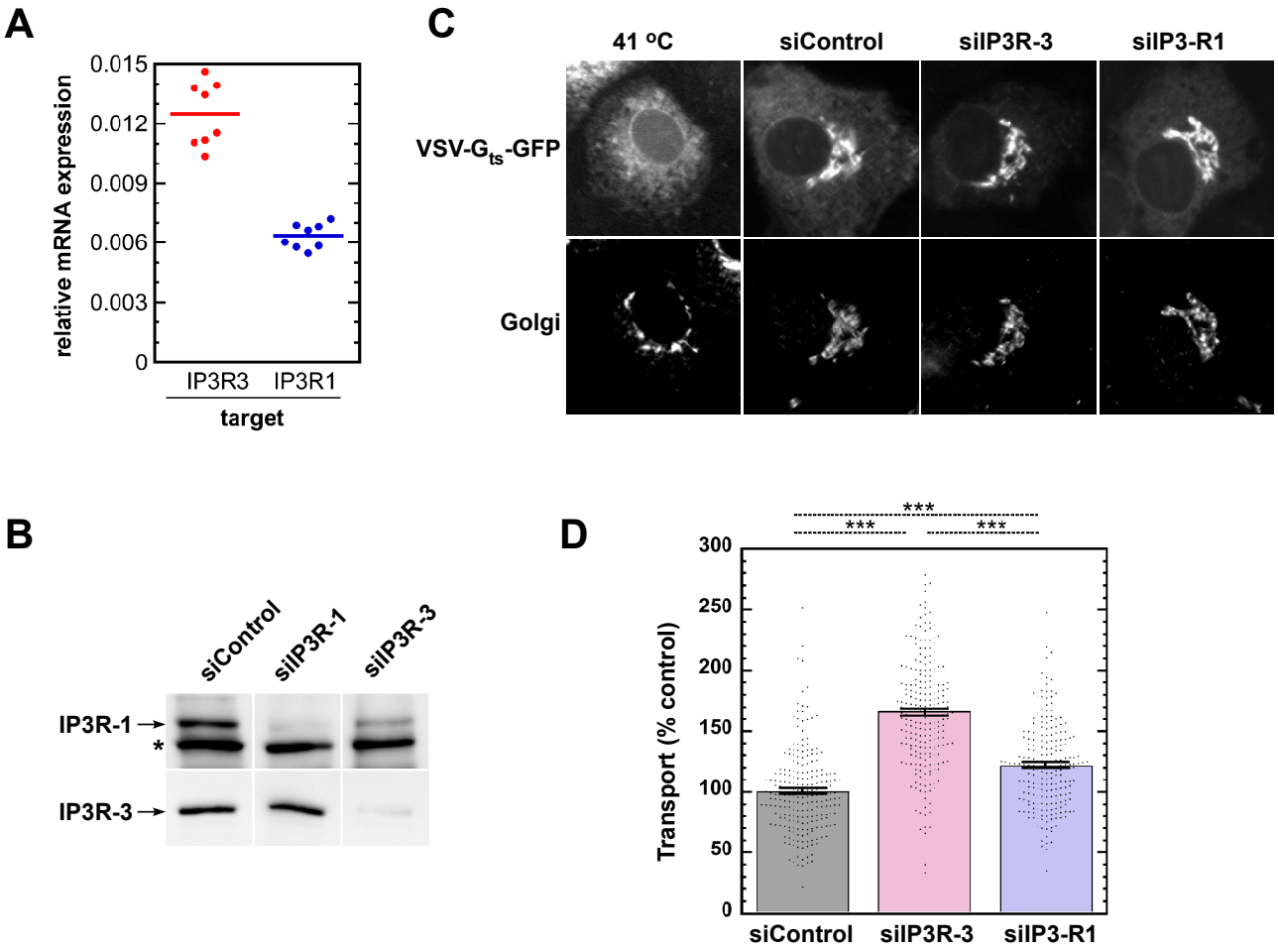

Figure 1. Expression of IP3 receptors regulates ER-to-Golgi transport in NRK cells. (A) Expression ratio of IP3R-1 and IP3R-3 in NRK cells analyzed by qRT-PCR. The quantity of each target RNA is normalized to that determined for GAPDH in parallel reactions. **(B)** Verification by immunoblot of IP3R depletions using isoform-specific siRNAs. Asterisk marks an unknown nonspecific band recognized by the anti-IP3R-1 antibody. **(C)** Representative images of NRK cells from the ER-to-Golgi transport assay quantified in D. NRK cells were transfected with VSV-G_{ts045}-GFP with or without siRNAs as indicated. Following growth at 41 °C for 48 h, cells were shifted to 32 °C for 10 min, to permit transport, prior to fixation. Fixed cells were immuno-labeled with mannosidase II and imaged by widefield microscopy; VSV-G-GFP and mannosidase II channels are displayed for each cell. **(D)** Each transfected cell was assigned a transport index representing trafficking of VSV-G based upon the ratio of Golgi to peripheral green fluorescence. The transport index of each individual cell is plotted. 200-300 cells were randomly quantified from each condition, and results shown are representative of at least 3 experiments with consistent trends. p-values for two-tailed Student T-tests with unequal variance are indicated above; * = $p \leq .05$; ** = $p \leq .005$; *** = $p \leq .0005$. Standard error is shown for each plot.

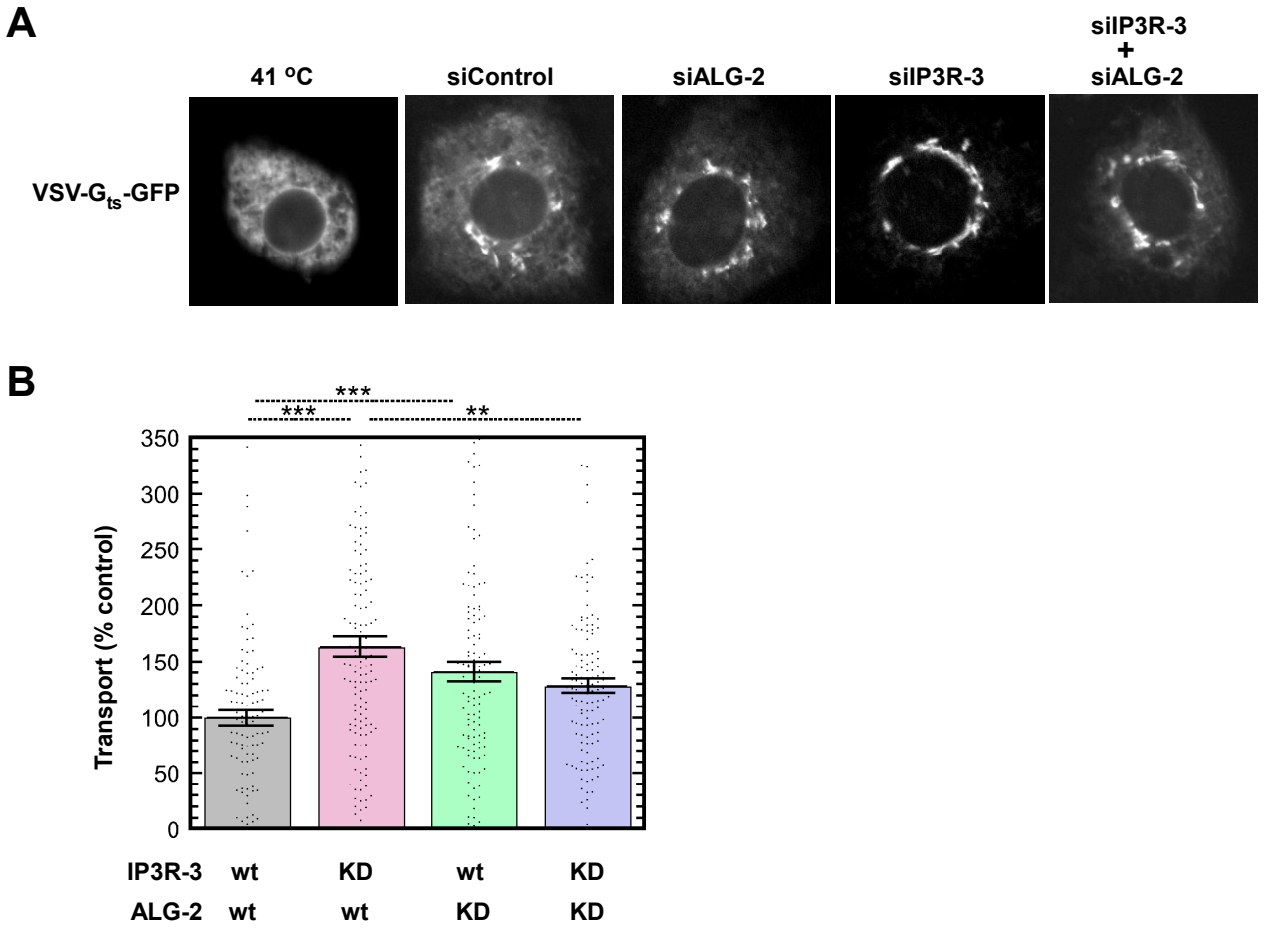

Figure 2. IP3R regulation of ER export requires ALG-2. In the absence of ALG-2, IP3R depletion fails to increase secretion. **(A)** Representative images of NRK cells from the ER-to-Golgi transport assay quantified in B (see Figure 1 legend for more detail); VSV-G-GFP is displayed for each representative cell. **(B)** Quantification of ≥100 cells for each condition from A (see Figure 1 legend for more detail).

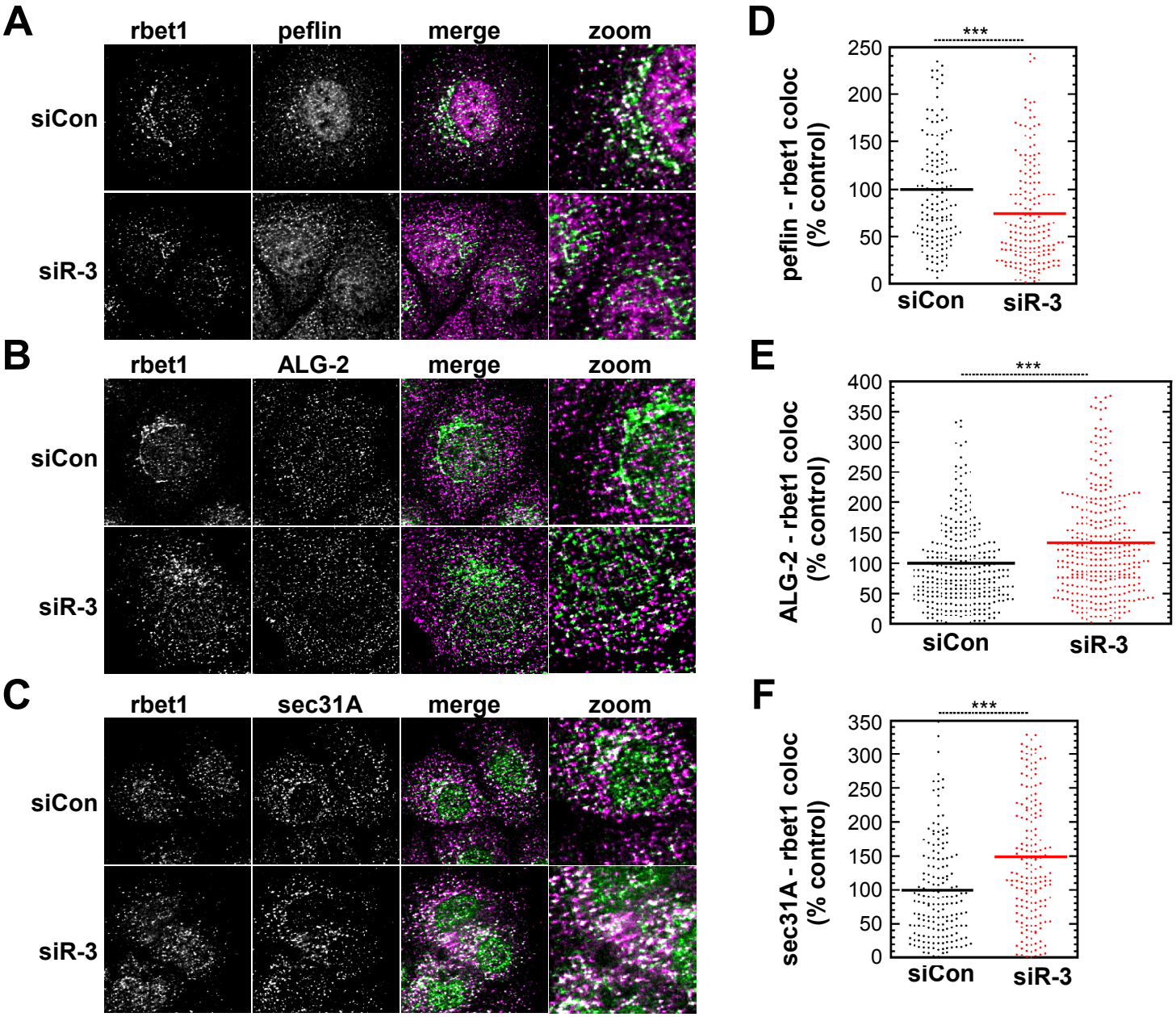

Figure 3. IP3R depletion causes a decrease in peflin and increases in ALG-2 and sec31A at ERES. (A-C) NRK cells were transfected with the indicated siRNAs. After 48 hrs, cells were fixed and immunolabeled for endogenous rbet1, peflin, ALG-2, or sec31A, as indicated. Representative micrographs are shown. **(D-F)** Object analysis on ~150 cells (D, F) or ≥300 cells (E) per condition to quantify overlap between rbet1 objects and the other labeled proteins.

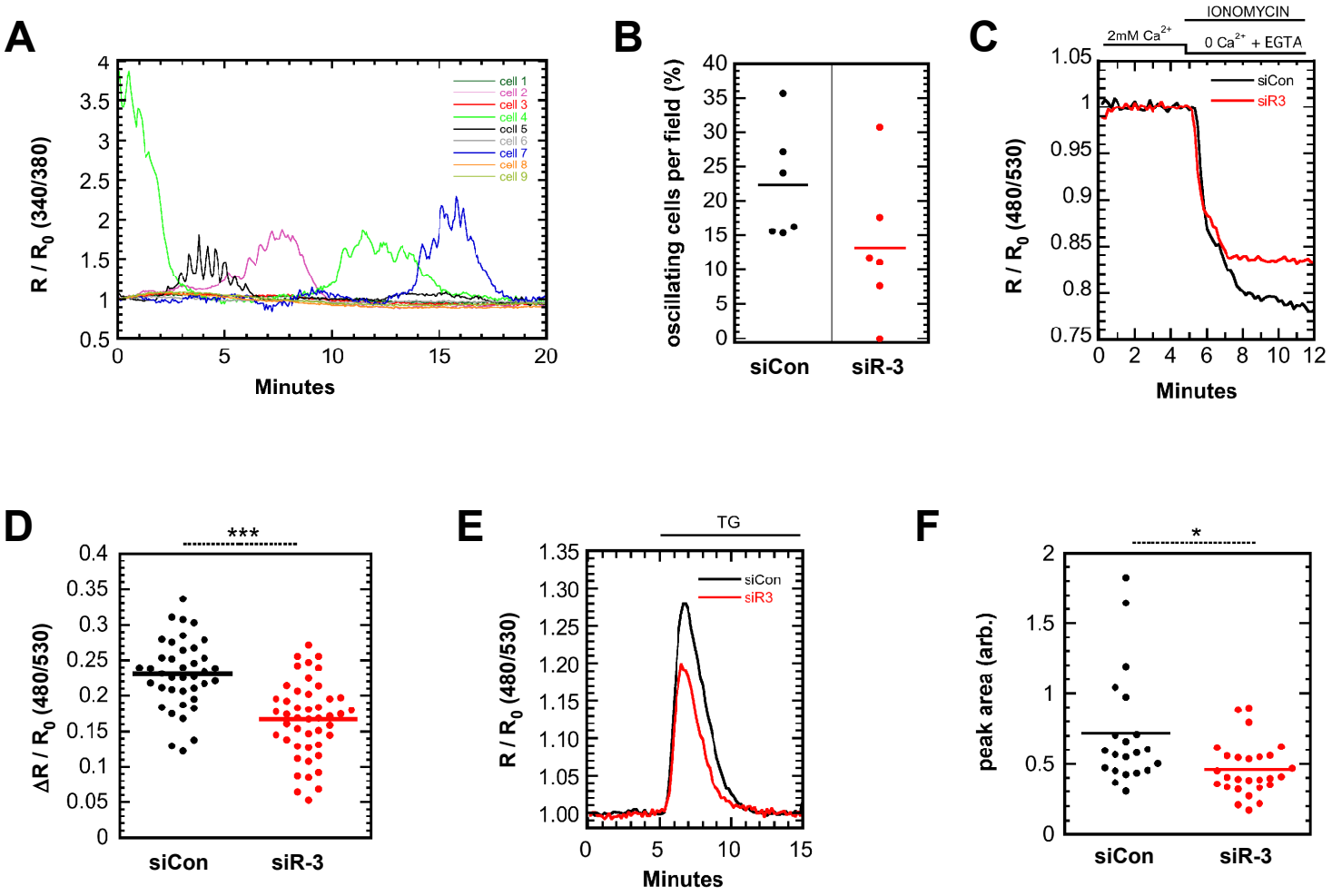

Figure 4. IP3R depletion causes reduced spontaneous Ca^{2+} oscillations and reduced ER luminal Ca^{2+} stores. (A) FURA-2 cytosolic Ca^{2+} recording of 9 control NRK cells in one field under steady-state conditions. Four cells displayed spontaneous Ca^{2+} signaling while five remained inactive. **(B)** Quantitation of six fields each of at least 10 cells each of control and IP3R-depleted cells recorded similarly to in A, except that the recording window was 10 min. Each cell was scored as either oscillating or inactive, and the fraction of oscillating cells per field is displayed. **(C)** Representative traces of ER luminal Ca^{2+}, using the sensor D1ER, upon depletion with ionomycin and low Ca^{2+} medium. **(D)** Quantitation of the luminal Ca^{2+} drops in many cells from three experiments of Ca^{2+} depletion traces as in C. **(E)** Representative traces of cytosolic Ca^{2+}, using the sensor D3cpv, upon release of luminal Ca^{2+} stores by addition of thapsigargin to the extracellular medium. **(F)** Quantitation of multiple cells from two experiments of the peak areas in traces as in E. In D and F, each dot represents one cell, whereas in B, each dot represents a field of ≥10 cells.

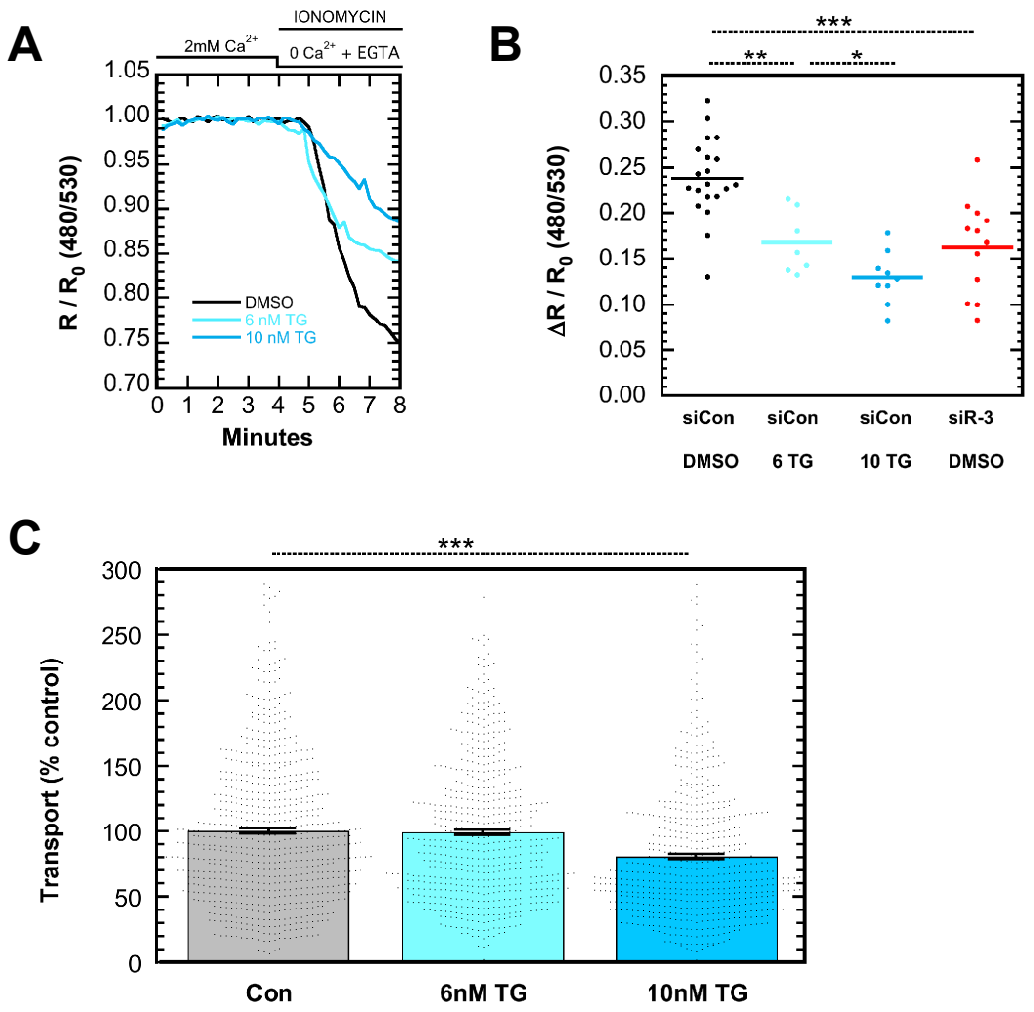

Figure 5. Partial depletion of luminal Ca^{2+} stores in the absence of IP3R siRNA does not increase ER export. (A) D1ER-transfected NRK cells were pretreated for 24 hrs with DMSO, 6 or 10 nM Tg, as indicated, and then depleted of ER luminal Ca^{2+} with ionomycin and low Ca^{2+} medium as in Figure 4. Shown are representative traces of the ER luminal Ca^{2+}drop as reported by D1ER. **(B)** 6 nM Tg lowers ER Ca^{2+} stores similarly to that of IP3R-3 siRNA. Cells were transfected with D1ER and an siRNA, and pretreated for 24 hrs with DMSO, 6 or 10 nM Tg, as indicated, and then depleted of ER luminal Ca^{2+} as in A. The luminal Ca^{2+} drops from individual cells in two experiments were quantitated and combined. (C) 6 nM Tg does not affect ER-to-Golgi transport rates, whereas 10 nM inhibits by 20%. NRK cells were transfected with VSV_{ts045}-G-GFP and pretreated with DMSO, 6 or 10 nM Tg, as indicated, and then ER-to-Golgi transport was measured as in Figures 1 and 2. Results from ≥600 cells per condition from several experiments are combined.

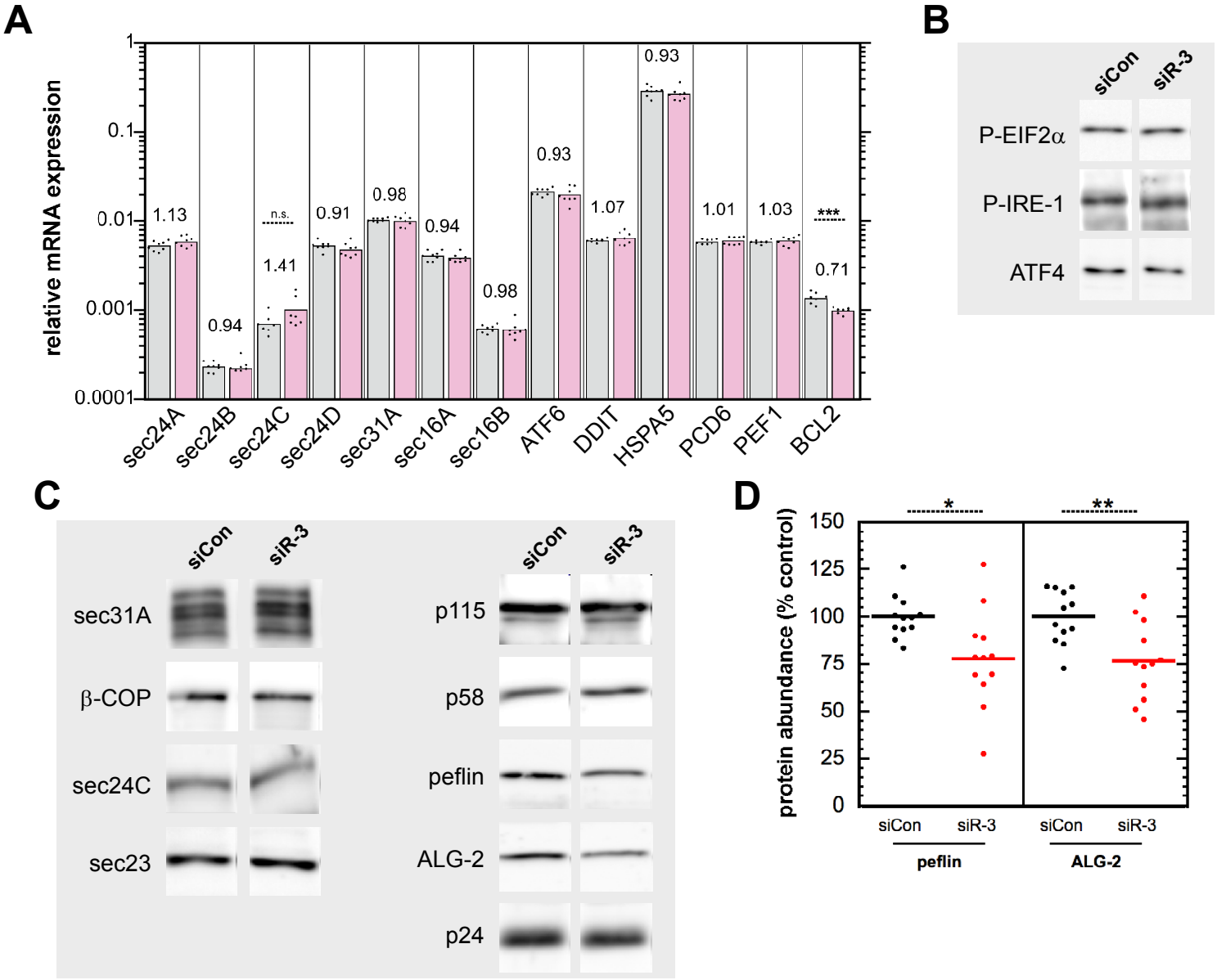

Figure 6. IP3R depletion destabilizes ALG-2 and peflin but does not affect expression of other ER export machinery. (A) NRK cells were transfected with control (gray) or IP3R-3 (light red) siRNAs, grown for 48 hrs, lysed and then mRNA was analyzed by qRT-PCR to detect expression of trafficking and other proteins. The quantity of each target RNA is normalized to that determined for GAPDH in parallel reactions. Value labels indicate the ratio of expression in siR-3 cells to that of control cells. **(B, C)** Immunoblots of ER stress proteins (B) and ER/Golgi trafficking machinery (C) in NRK cell extracts, 48 hrs after transfection with control or IP3R-3 siRNAs. No significant changes were observed, except for decreases in ALG-2 and peflin. **(D)** Quantitation of multiple technical replicates from several different experiments documented effects of IP3R depletion on ALG-2 and peflin protein abundance.